



Article

---

# BER Minimization by User Pairing in Downlink NOMA Using Laser Chaos Decision-Maker

---

Masaki Sugiyama, Aohan Li, Zengchao Duan, Makoto Naruse and Mikio Hasegawa

## Special Issue

Advances in Intelligence Networking and Computing


Edited by

Prof. Dr. Jong-Deok Kim, Prof. Dr. Mikio Hasegawa and Prof. Dr. Won-Joo Hwang



## Article

# BER Minimization by User Pairing in Downlink NOMA Using Laser Chaos Decision-Maker

Masaki Sugiyama <sup>1</sup>, Aohan Li <sup>1,\*</sup> , Zengchao Duan <sup>1</sup>, Makoto Naruse <sup>2</sup>  and Mikio Hasegawa <sup>1</sup> 

<sup>1</sup> Department of Electrical Engineering, Graduate School of Engineering, Tokyo University of Science, Tokyo 125-8585, Japan; 4318038@ed.tus.ac.jp (M.S.); sxytdzc@outlook.com (Z.D.); hasegawa@ee.kagu.tus.ac.jp (M.H.)

<sup>2</sup> Department of Information Physics and Computing, Graduate School of Information Science and Technology, The University of Tokyo, Tokyo 113-8656, Japan; makoto\_naruse@ipc.i.u-tokyo.ac.jp

\* Correspondence: aohanli@ieee.org

**Abstract:** In next-generation wireless communication systems, non-orthogonal multiple access (NOMA) has been recognized as essential technology for improving the spectrum efficiency. NOMA allows multiple users transmit data using the same resource block simultaneously with proper user pairing. Most of the pairing schemes, however, require prior information, such as location information of the users, leading to difficulties in realizing prompt user pairing. To realize real-time operations without prior information in NOMA, a bandit algorithm using chaotically oscillating time series, which we refer to as the laser chaos decision-maker, was demonstrated. However, this scheme did not consider the detailed communication processes, e.g., modulation, error correction code, etc. In this study, in order to adapt the laser chaos decision-maker to real communication systems, we propose a user pairing scheme based on acknowledgment (ACK) and negative acknowledgment (NACK) information considering detailed communication channels. Furthermore, based on the insights gained by the analysis of parameter dependencies, we introduce an adaptive pairing method to minimize the bit error rate of the NOMA system under study. The numerical results show that the proposed method achieves superior performances than the traditional using pairing schemes, i.e., Conventional-NOMA pairing scheme (C-NOMA) and Unified Channel Gain Difference pairing scheme (UCGD-NOMA), and  $\epsilon$ -greedy-based user pairing scheme. As the cell radius of the NOMA system gets smaller, the superior on the BER of our proposed scheme gets bigger. Specifically, our proposed scheme can decrease the BER from  $10^{-1}$  to  $10^{-5}$  compared to the conventional schemes when the cell radius is 400 m.

**Keywords:** non-orthogonal multiple access (NOMA); user pairing; laser chaos decision-maker; bandit algorithm; system optimization; adaptive control; bit error; ACK; NACK



**Citation:** Sugiyama, M.; Li, A.; Duan, Z.; Naruse, M.; Hasegawa, M. BER Minimization by User Pairing in Downlink NOMA Using Laser Chaos Decision-Maker. *Electronics* **2022**, *11*, 1452. <https://doi.org/10.3390/electronics11091452>

Academic Editor: Christos J. Bouras

Received: 1 April 2022

Accepted: 26 April 2022

Published: 30 April 2022

**Publisher's Note:** MDPI stays neutral with regard to jurisdictional claims in published maps and institutional affiliations.



**Copyright:** © 2022 by the authors. Licensee MDPI, Basel, Switzerland. This article is an open access article distributed under the terms and conditions of the Creative Commons Attribution (CC BY) license (<https://creativecommons.org/licenses/by/4.0/>).

## 1. Introduction

Innovative wireless technologies are highly demanded to meet the huge demands of various services and the fast growth of the mobile Internet and Internet of Things (IoT) applications [1–5]. Non-orthogonal multiple access (NOMA) is an indispensable technology in next-generation wireless systems, achieving manifold capacity gains because of its advantages such as high spectral efficiency, improved cell-edge throughput, low transmission latency, large connection capacity, high achievable data rate and so on [6–9].

In NOMA, the basic idea is to serve multiple users or devices in the same resource block. Since the signals of multiple users are superimposed in the power domain, the receivers conduct multiuser-detection (MUD) algorithms, such as successive interference cancellation (SIC), to identify individual signals [10–12]. In NOMA systems, user pairing and resource allocation are important to achieve its potential communication performances [13,14]. In the present study, we focus on user pairing and assume that the

number of multiple users in the same resource block simultaneously is two. Hence, precisely, user pairing herein means combining two users to share the same resource block. In NOMA systems, the performance varies depending on user pairings; for instance, signal-to-interference-plus-noise ratio (SINR), throughput, and so on [15,16]. Thus, the pairing scheme is important and attracts increased attention.

There are several studies for pairing schemes, e.g., conventional NOMA (C-NOMA) [17] and uniformed channel gain difference-NOMA (UCGD-NOMA) [18]. The basic concept of C-NOMA and UCGD-NOMA is to pair faraway users with nearby users. In these two methods, users are first divided into two categories based on their distances from the base station: “near area” and “far area”. C-NOMA is the pairing scheme, which pairs the nearest user to the base station in the near area with the farthest user to the base station in the far area, the second-nearest user in the near area with the second-farthest user in the far area. Other users are paired similarly. UCGD-NOMA is the pairing scheme, which pairs the user who is the nearest to the base station in the near area with the user who is the nearest to the base station in the far area, the second-nearest user in the near area with the second-nearest user in the far area, and so on. Likewise, other users are paired. However, these fixed pairing schemes based on distances need exact location information for pairings and may not achieve the optimal user pairing. Consequently, these pairing schemes may find it difficult to achieve optimal and fast user pairing. In [19], user grouping is followed by user pairing. That is, users are first divided into clusters based on channel gains, then user pairing is performed for each cluster. However, obtaining channel information and the two-stage user pairing process may bring extra communication and decision delay. To fully utilize the potential of NOMA and reduce the communication delay, a highly efficient and fast pairing scheme is demanded. Indeed, machine learning approaches, such as reinforcement learning and deep learning, are examined for NOMA systems [20–23]. In [20–22], Q-learning or deep Q-learning has been implemented to NOMA. In [23], user pairing and resource allocation are based on deep learning. In [24], the deep learning method using long short-term memory (LSTM) network has been applied to NOMA systems. However, state information, such as the location of the users, is still necessary to implement these machine learning methods, which may lead to extra communication and decision delays when obtaining state information. Hence, the above-mentioned methods also face difficulties in realizing high-speed and real-time processing in view of future dynamic environments.

In the meantime, optics and photonics have been intensively studied for accelerating computing, especially machine learning applications [25–28]. Laser chaos has been known to produce ultrafast irregular time series [29], which is applied for reinforcement learning applications [30–32]. In [30], the two-armed bandit problems are successfully solved at the GHz order by utilizing laser chaos time-series; we call such a system the laser chaos decision-maker, hereafter. Moreover, Okada et al. clarified that the time-domain correlation inherent in laser chaos leads to acceleration in solving bandit problems [33]. The scalability of such a laser chaos decision-maker to multi-armed bandit (MAB) problems has been studied by constructing tree structures [31]. MAB is a machine learning framework in which an agent has to select actions (arms) in order to maximize its cumulative reward in the long term [34]. The applications of laser chaos decision-maker to wireless communications have been studied to exploit its superior adaptation ability [16,35,36]. In [35], a dynamic channel selection problem in a wireless local area network (precisely, selecting one channel from four available channels in IEEE802.11a) was examined experimentally by transforming the problem into a MAB problem. The laser-chaos-based MAB algorithm successfully demonstrated autonomous and adaptive channel selection, wherein a high throughput of more than 10 Mbps was accomplished between terminals and the access points under dynamically changing network traffic. The MAB algorithm is an algorithm that tries to balance “explore” and “exploit” to select a slot machine with a high reward probability in the MAB problem [37]. In [36], a laser chaos decision-maker was utilized to perform dynamic channel bonding in an IEEE802.11ac network. Here, the arms correspond to the channel bonding configurations. Autonomous and adaptive channel bonding was

experimentally demonstrated, achieving better performances in terms of throughput than other reinforcement learning methods such as  $\epsilon$ -greedy and Upper Confidence Bound (UCB) 1-tuned.

In [16], a pairing scheme was examined using the laser-chaos-based MAB algorithm where the arms are associated with the possible pairing. That is, the reward of each arm is associated with the throughput of the corresponding pairing. It should be noted that the location information of the users is not utilized. An optimal or near-optimal pairing was promptly realized. The fast adaptation ability is expected to offer the capability to be adapted to dynamic environmental changes such as user mobility. In [16], however, the user pairing is conducted based on the estimated throughput of the channels, meaning that the detailed actual communication system was not taken into account. For example, modulation methods and responses by users during communications, such as acknowledgment (ACK) information, among others, were not considered. Thus, the performance in NOMA systems may not be correctly evaluated, and the route to actual implementation should be investigated.

In this study, we examine a user pairing scheme for NOMA systems based on the laser chaos decision-maker while considering the bit error rate (BER) of the communication channels and user responses on the basis of a realistic system model. The reason that we introduce a laser chaos decision-maker to the user-pairing problem for NOMA systems is that a laser chaos decision-maker can make decisions at a high speed without prior information. Hence, a laser chaos decision-maker-based user pairing scheme can realize real-time operations without prior information in NOMA. Moreover, the reason that we consider the details of the real communication system, e.g., BER of the communication channels, user responses, error correction code, modulation, etc., is that we would like to enable our proposed scheme to be used in real communication systems. Herein, downlink data transfer is investigated; we assume that the base station owns a laser chaos decision-maker, taking the role of user pairing. The users or terminals send back ACK signals to the base station if they succeed in receiving the data from the base station. The aim of the base station is to find the pairing that minimizes BER of the entire system under study. In addition, by examining detailed parameter dependencies in the pairing by laser chaos decision-maker, we introduce an adaptive scheme to optimize the operation parameters in the NOMA system. Moreover, the performance achieved by the proposed method is compared with C-NOMA, UCGD-NOMA, and  $\epsilon$ -greedy-based user pairing in terms of BER, where the proposed method accomplishes superior BER than the counterparts. The main contributions of this paper can be summarized as follows:

- We design a fast user-pairing scheme that can make real-time decisions for downlink NOMA systems based on the laser chaos decision-maker while considering the BER of the communications and user responses on the basis of a realistic system model.
- To improve the performance in terms of BER for our proposed scheme, error-correcting codes are introduced in the system. In addition, parameter dependencies in the user pairing by laser chaos decision-maker are investigated to minimize the BER of the NOMA system. Simulation results indicate that our proposed scheme can improve the BER of the NOMA system.
- To verify the effectiveness of the proposed scheme, we conduct a performance evaluation for our proposed scheme and compare it to several other conventional schemes. Simulation results demonstrate that our proposed scheme exhibits superior performances in BER compared to other conventional schemes. As the cell radius of the NOMA system gets smaller, the superior on the BER of our proposed scheme gets bigger. Specifically, our proposed scheme can decrease the BER from  $10^{-1}$  to  $10^{-5}$  compared to the conventional schemes when the cell radius is 400 m.

The rest of the paper is organized as follows. After describing the system model of the present study in Section 2, Section 3 introduces the laser chaos decision-maker. Section 4 presents the proposed method and shows basic numerical results. Section 5 investigates

parameter dependencies and discusses performance optimization. Section 6 concludes the paper.

## 2. System Model and Problem Formulation

In this paper, we consider a downlink single-cell NOMA system with one base station (BS) and multiple users. Figure 1 shows an overview of the NOMA system model considered in this study. We assume that the BS and all of the users have one antenna each. BS sends data to the users, and the users respond with ACK or NACK (negative acknowledgment) information to BS when the downlink data transfer is successful and non-successful, respectively.

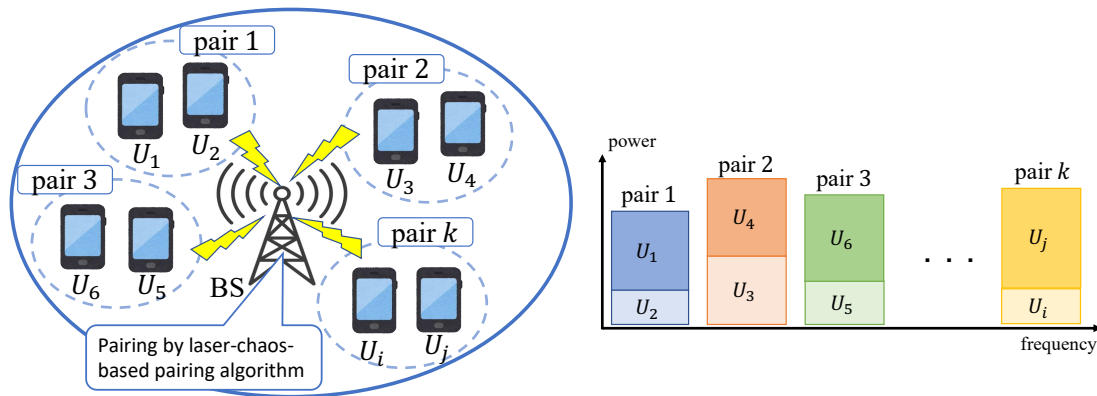


**Figure 1.** System model.

The outline of how the system works is described as follows. First, BS determines certain user pairings and transmits data to the users based on the determined pairing. The users receive and decode the data, followed by checking bit errors and sending a response to BS with ACK or NACK according to the bit errors. Next, BS updates user pairing based on the received ACK and NACK information. BS transmits data to users again based on the revised pairing. By repeating above processes, BS aims to achieve an optimal pairing to minimize BER in the NOMA system.

Let  $U = \{U_1, U_2, \dots, U_i, \dots, U_j, \dots, U_N\}$  be the set of  $N$  users in a circular cell and  $K = \{1, 2, \dots, k, \dots, N/2\}$  be the index of each pair.  $N$  is the total number of users, which we assume is an even number. The total bandwidth is assumed to be  $B$ . We assume that the bandwidth for each pair is equal. Then, the bandwidth for the  $k$ th pair can be represented as  $B_k = B/(N/2)$ . The NOMA symbol  $x_k$  to the  $k$ th pair can be expressed as follows [38]:

$$x_k = \sqrt{a_k P_k} x_k^i + \sqrt{(1 - a_k) P_k} x_k^j, \quad (1)$$

where  $x_k^i$  and  $x_k^j$  are the signals for the  $i$ th and  $j$ th users that from the pair  $k$ .  $x_k^i$  and  $x_k^j$  are  $\theta_i$  and  $\theta_j$  modulated by a certain modulation method and turned into OFDM symbols by IFFT, where  $\theta_i$  and  $\theta_j$  are data bit of the  $i$ th and  $j$ th users.  $a_k$  is the power allocation factor for the  $k$ th pair. We assume that the  $i$ th user is located closer to the BS than the  $j$ th user.  $P_k$  is the transmit power allocated to each pair for the  $k$ th pairs. The received signal  $y_n$  at the  $n$ th user in the  $k$ th pair can be expressed as follows [38]:

$$y_n = d_n^{-\lambda} h_n x_k + w_n, \quad (2)$$

where  $d_n^{-\lambda}$  is the path loss between the BS and the  $n$ th user and  $\lambda$  is the path-loss exponent,  $h_n$  is the Rayleigh fading of the  $n$ th, and  $w_n$  is the additive white Gaussian noise (AWGN) with zero mean and variance of  $\sigma_n^2$ .  $\sigma_n^2$  can be expressed as  $\sigma_n^2 = N_0 B_k$ , where  $N_0$  is the noise power spectral density. Herein, we assume that the farthest user in the  $k$ th user pairing is

the  $f$ th user. Then, the signal-to-noise ratio (SNR) of the farthest user  $U_f$  can be expressed as follows:

$$\text{SNR}_f = \frac{|\tilde{h}_f| d_f^{-\lambda} (1 - a_\kappa) P_\kappa}{|w_f|}. \quad (3)$$

In this study, a laser chaos decision-maker is used in the BS to pair users. The object of our proposed scheme is to minimize the BER of the NOMA system by optimizing user pairing, which can be expressed as follows:

$$\min_v \frac{\sum_{n=1}^N \text{bit-error}_n}{\sum_{n=1}^N \theta_n}, \quad (4)$$

where  $\text{bit-error}_n$  denotes the number of bit errors at the  $n$ th user.  $v$  denotes the user pairing combinations, which will be explained in Section 4.

### 3. The Principle of Laser Chaos Decision-Maker

Here, we review the principle of the laser chaos decision-maker, which is an ultrafast photonic reinforcement learning method based on laser chaos. The details can be found in [30,31].

When a portion of the output light from a laser is fed back to the laser cavity after a certain delay via an externally arranged mirror, instability of the laser is induced, leading to chaotic oscillatory behavior [30]. Figure 2 shows the decision making based on laser chaos time-series produced by a semiconductor laser [32]. The principle of decision-making based on laser chaos is summarized as follows. By comparing the sampled amplitude of the laser chaos time-series with the threshold value, a decision on the slot machine selection is made. Here we consider a two-armed bandit problem where the issue is to promptly and accurately find the higher reward probability slot machines. The two slot machines are called machine 0 and machine 1. If the sampled amplitude of the laser chaos time series is greater than or equal to the threshold value, slot machine 0 is selected. Otherwise, the decision is to choose slot machine 1. The threshold is adjusted according to the reward from the selected slot machine (in other words, win or lose) so that the slot machine with the higher reward probability will be selected in the subsequent trials.

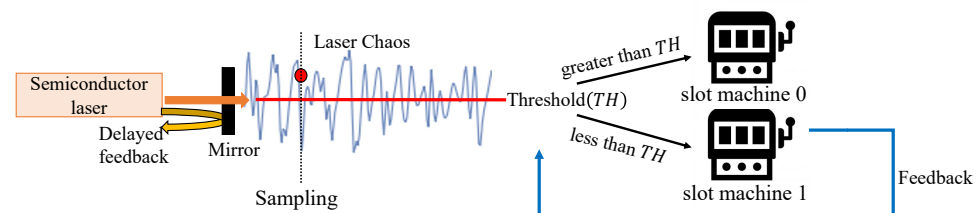


**Figure 2.** Architecture of laser chaos decision-maker for two-armed bandit problems [30].

More precisely, the threshold value  $TH(t)$  at step  $t$ , which is used in the comparison with the laser chaos signal level, is given as follows:

$$TH(t) = k \times \lfloor TA(t) \rfloor \quad (5)$$

where  $TA(t)$  is the threshold adjuster value at step  $t$ ,  $\lfloor TA(t) \rfloor$  is the nearest integer to  $TA(t)$  rounded to zero and  $k$  is a constant to control the range of  $TH(t)$ . The value of  $\lfloor TA(t) \rfloor$  can be one of the values in  $-Z, \dots, -1, 0, 1, \dots, Z$ , where  $Z$  is a natural number. Thus, the number of thresholds is  $2Z + 1$ .  $TH(t)$  is limited to the range of  $-kZ$  to  $kZ$  because of setting  $\lfloor TA(t) \rfloor = Z$  when  $\lfloor TA(t) \rfloor$  is greater than  $Z$ , as well as  $\lfloor TA(t) \rfloor = -Z$  when  $\lfloor TA(t) \rfloor$  is less than  $-Z$ . The threshold adjuster  $TA(t)$  is updated according to the following [30,31]:



$$TA(t+1) = \begin{cases} \pm\Delta + \alpha TA(t), & \text{if selected slot machine wins.} \\ \mp\Omega + \alpha TA(t), & \text{if selected slot machine loses.} \end{cases} \quad (6)$$

where  $\alpha$  ( $0 \leq \alpha \leq 1$ ) is the forgetting rate to control the influence of past experiences,  $\Delta$  is the certain increment and  $\Omega$  is the increment parameter. In the case that the selected slot machine wins, i.e., if a reward is obtained by playing the selected slot machine, the threshold adjustment value  $TA(t)$  is updated by  $\pm\Delta + \alpha TA(t)$ . Otherwise, the selected slot machine loses, i.e., a reward is not obtained by playing the selected slot machine; the threshold adjustment value  $TA(t)$  is updated by  $\mp\Omega + \alpha TA(t)$ .  $\Omega$  is the increment parameter based on the history of choices and benefits. We define that  $S_i$  and  $L_i$  is the number of times that slot machine  $i$  is selected and that of wins by playing the selected slot machine  $i$  until step  $t$ , respectively. At this time, the estimated reward probability of the  $i$ th slot machine  $P_i$  is given by:

$$P_i = \frac{L_i}{S_i}. \quad (7)$$

In the two-armed bandit problem, we use the estimated reward probability in Equation (7) to define  $\Omega$  as follows:

$$\Omega = \frac{P_0 + P_1}{2 - (P_0 + P_1)}, \quad (8)$$

where  $P_0$  and  $P_1$  are the estimated reward probabilities of the two slot machines with the highest estimated reward probability and the second-highest estimated reward probability, respectively.

By cascading the above-described algorithm, the scalability of the laser chaos decision-maker is realized [31]. By arranging pipelined thresholds, we can choose one among multiple slot machines. Figure 3 illustrates the scalable decision-making utilizing laser chaos time-series. More concretely, scalable decision-making follows the rule below. At step  $t_1$ , the level of chaotic output  $s(t_1)$  is compared to the threshold  $TH_1$ . At step  $t_2$ , the level of chaotic output  $s(t_2)$  is compared to the threshold  $TH_{2,1}$ , if  $s(t_1)$  is greater than or equal to  $TH_1$ . Otherwise,  $s(t_2)$  is compared to the threshold  $TH_{2,2}$ . Similarly, at step  $t_3$ ,  $s(t_3)$  is compared with either  $TH_{3,0,0}$ ,  $TH_{3,0,1}$ ,  $TH_{3,1,0}$ , or  $TH_{3,1,1}$ . In this manner, comparisons with the chaotic signals and multiple threshold continue until a slot machine is selected. Thus, comparisons with the chaotic signals and multiple thresholds allow scalable decision making.

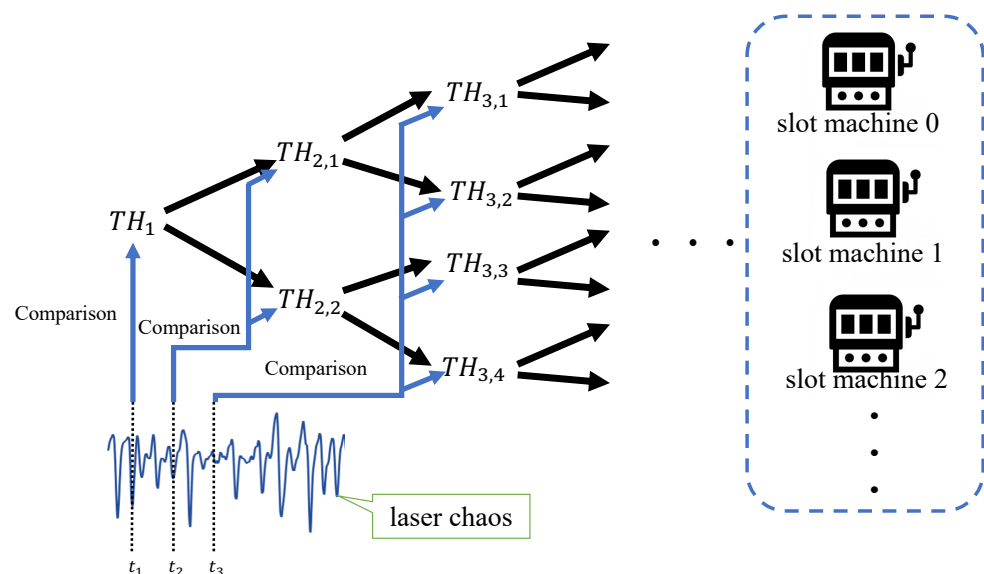


Figure 3. Scalable decision-making by a hierarchical architecture [31].

#### 4. User Pairing in NOMA System with Laser Chaos Decision-Maker (LCDM-NOMA)

Here, we introduce the proposed user pairing method for the NOMA system with laser chaos decision-maker, which we call LCDM-NOMA hereafter. First, we explain the operating principle of the proposed method in Section 4.1. Then, we demonstrate the simulation results of the proposed method in Section 4.2.

##### 4.1. Operating Principle

Here, we explain the system behavior with the laser chaos decision-maker in detail and the definition of the concepts, e.g., reward, used to operate the laser chaos decision-maker. In this study, user pairing is decided by the BS using a laser chaos decision-maker aiming to accomplish the optimal communication performance, i.e., minimizing BER. The outline of the proposed scheme is shown in Figure 4, and is described as follows.

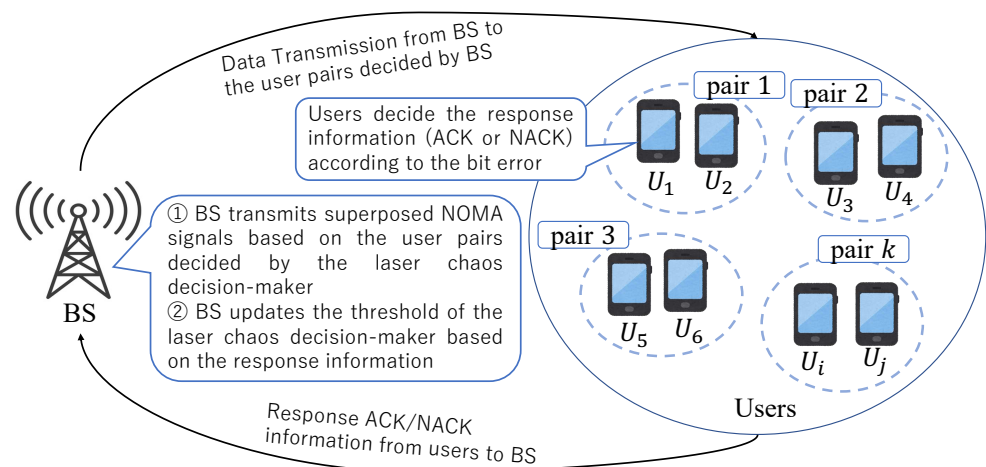


Figure 4. Outline of the proposed user pairing scheme.

As shown in Figure 4, the BS firstly decides the pairing options by the laser chaos decision-maker and transmits data to the users based on the decided user pairing options. Then, BS receives feedback information, i.e., ACK information and NACK information from the users. Next, thresholds regarding the laser chaos decision-maker are updated according to the feedback. Figure 5 shows the configuration of the laser chaos decision-maker for user pairing in NOMA, where the arms in the MAB problem are associated with the pairing options. The pairing options are selected by comparing the sampled amplitude from the laser chaos time series with threshold values. The threshold is adjusted according to the feedback of the selected pairing option. In Figure 5,  $PO_v$  denotes the  $v$ th user pairing option. The pairing options are distinguished by the index, which is represented by a binary code  $I_1 I_2 \dots I_M$  with  $I_i$  ( $i = 1, 2, \dots, M$ ) being 0 or 1, where  $M$  is a natural number and  $I_1$  is the most significant bit (MSB) and  $I_M$  is the least significant bit (LSB). The index represented by the  $v$ th pairing option  $PO_v$  and the corresponding binary code is the same binary code as the binary representation of  $v$ . For instance, the binary representation of the 4th pairing option  $PO_4$  is 0100, which is 4 in 10 hex.

For intuitive understanding, Figure 6 illustrates an example when the number of users is six in a NOMA system. In this case, the number of pairing options is 15. Hence,  $M = 4$  with  $I_1 I_2 I_3 I_4 = \{0000, 0001, 0010, \dots, 1111\}$  can accommodate 15 pairing options.  $I_1$ ,  $I_2$ ,  $I_3$  and  $I_4$ , respectively indicates the MSB, the second MSB, the third MSB and the least significant bit. The pairing option  $PO_0$  is associated with 0000,  $PO_1$  is associated with 0001 and other pairing options are associated as well. By adjusting the threshold  $TH_{3,1,1,1}$ , the “null” option, corresponding to the index 1111 in Figure 6 is never selected; hence, the laser chaos decision-maker selects the pairing option among  $PO_0$  to  $PO_{14}$ . The index of the pairing option to be selected is decided bit by bit from MSB to the least significant bit in the pipeline rule.



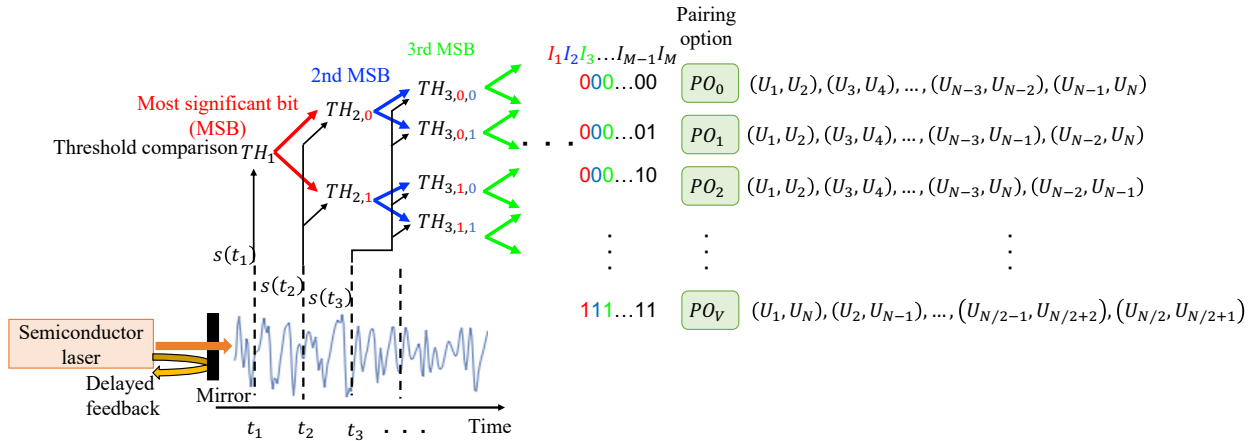


Figure 5. User pairing using the laser chaos decision-maker.

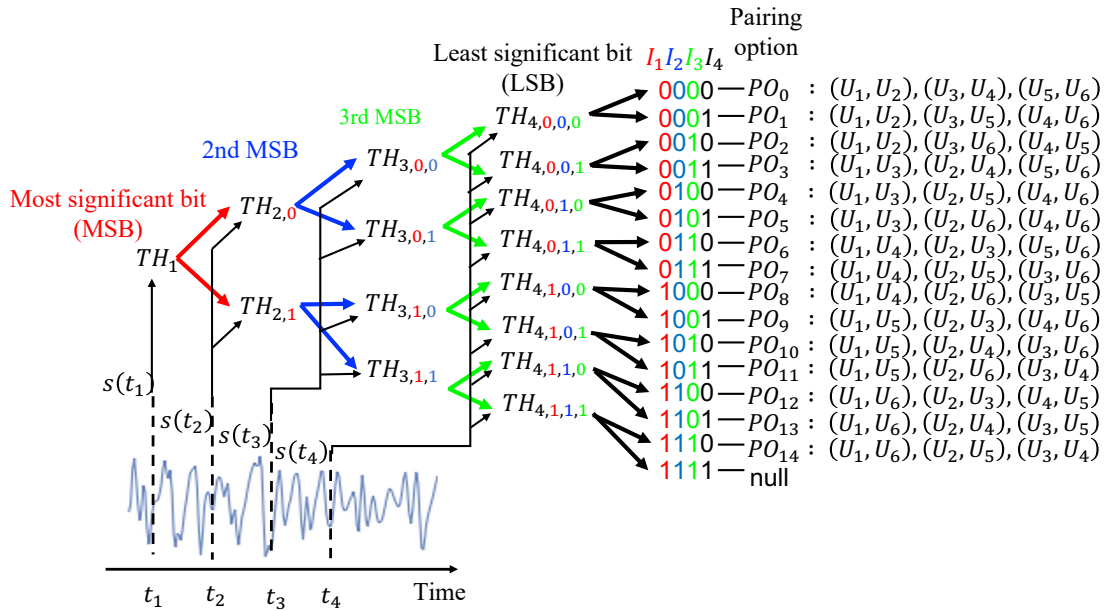


Figure 6. User pairing using the laser chaos decision-maker in the NOMA system in the case of 6 users.

For each of the bits, the decision is made based on a comparison between the sampled amplitude of the laser chaos time-series and the specified threshold value. First, the level of chaotic output  $s(t_1)$  measured at  $t = t_1$  is compared to a threshold value given as  $TH_1$ . The output of the comparison is instantly the decision of the MSB related to selecting the pairing option. If  $s(t_1)$  is larger than or equal to  $TH_1$ , the MSB of the pairing option is decided to be 0, which we donate as  $I_1$  (MSB) = 0. Otherwise, the MSB is decided as 1 ( $I_1 = 1$ ). Based upon the decision of the MSB, the sampled amplitude of the laser chaos time-series  $s(t_2)$ , measured at  $t_2$ , is compared to another threshold value denoted as  $TH_{2,0}$  or  $TH_{2,1}$ . In the case of  $I_1 = 0$ ,  $s(t_2)$  is compared to  $TH_{2,0}$ . The first number two in the  $TH_{2,0}$ 's subscript states corresponds to the second MSB, and the second number zero in the subscript states corresponds to the value of the  $I_1$ . If  $s(t_2)$  is greater than or equal to the threshold  $TH_{2,0}$ , the second MSB is set to be zero, i.e., ( $I_2 = 0$ ), otherwise it is set to be one, i.e., ( $I_2 = 1$ ). In these rules, the threshold value comparison finishes when all  $M$  bits information of the specified option are decided. The update formula of the threshold adjuster value  $TA$  can be expressed as follows [30,31]:

$$TA_{L,I_1,I_2,\dots,I_{(L-1)}}(t+1) = \begin{cases} \pm\Delta + \alpha TA_{(L,I_1,I_2,\dots,I_{(L-1)})}(t), & \text{if selected slot machine wins.} \\ \mp\Omega_{L,I_1,I_2,\dots,I_{(L-1)}} + \alpha TA_{L,I_1,I_2,\dots,I_{(L-1)}}(t), & \text{if selected slot machine loses.} \end{cases} \quad (9)$$

where  $\Delta$  is a constant and  $\Omega_{L,I_1,I_2,\dots,I_{(L-1)}}$  can be calculated using Equation (8).  $L$  corresponds to the  $L$ th MSB.  $L$  is  $1 \leq L \leq M$  and  $I_0$  is not described.

After determining the pairing based on the above algorithm, BS transmits data to users based on the determined pairing. The users check bit errors after decoding the received data. The users send back ACK or NACK signals to BS as the following. If bit errors do not occur, the users send ACK to BS. Otherwise, bit errors occur and the users transmit NACK to BS. Finally, BS gets a reward or non-reward according to the number of ACKs received.

If the total amount of ACKs received at the base station is greater than or equal to  $X$ , we assume that BS gets a reward (win), otherwise gets a no-reward (lose). Here,  $X$  is defined as the reward judgment factor. The threshold value is updated by updating the threshold adjuster value in Equation (10). After the update, BS generates the next user pairing and transmits data to users again. Receiving and decoding data, users check bit errors and respond ACK or NACK to BS. BS updates the threshold of the laser chaos decision-maker. By repeating these processes, the BS searches for the optimal pairing.

#### 4.2. Performance Evaluation

We present the numerical results to evaluate the performance in terms of BER using MATLAB R2021a. In our simulation, we consider 5G macro-cell and micro-cell, where the path-loss exponent and the propagation conditions are set as 3 and non-line-of-sight [22]. We consider 10 users ( $N = 10$ ) and a circular cell where users are arranged randomly. The path-loss exponent is set as 3.0. The power allocation is fixed; all pairs are allocated 20 dBm regardless of the pairing option, and the power allocation factor is  $a_k = 0.1$ , for all  $k$  ( $k = 1, 2, \dots, N/2$ ). The average received signal-to-noise ratio (SNR) of the farthest user is summarized in Table 1. The forgetting rate  $\alpha$  is 1.0 and  $\Delta$  is 1.0. The number of bits sent to each user is 256.  $x_k^i$  and  $x_k^j$  is a signal of “data bit per user” modulated by QPSK and transformed into OFDM symbols by IFFT. The parameter settings in the performance evaluation related to the NOMA systems refer to [39], which are summarized in Table 2.

**Table 1.** The average received SNR of the farthest user.

Cell Radius [m]	100	200	300	400	500	600	700	800	900	1000
SNR [dB]	74.8	65.8	60.5	56.7	53.8	51.4	49.5	47.7	46.2	44.8

**Table 2.** Parameter Settings.

Parameter	Value
Number of users	10
Cell shape	Circular
Deployment of users	Uniform distribution
Path-loss exponent	$\lambda = 3.0$
Propagation condition	Non-line-of-sight propagation
Transmission power allocated to each pair	$P_k = 20$ dBm
Power allocation factor for the $k$ th pair	$a_k = 0.1, \forall k$
Noise power spectral density	$-170$ dBm
Total bandwidth	$B = 5$ MHz
Reward criterion based on the number of receipt ACK information	$X = 10$ (equal to the number of users)
Forgetting rate	$\alpha = 1.0$
Number of bits sent to each user	$\theta_n = 256$ bit, $\forall n$

First, we visualize the behavior of the laser chaos decision-maker. Figure 7a shows an evolution of the actually selected pairing option index as a function of time, where the pairing is not settled initially but stabilized after approximately 1000 steps. More precisely, the proposed method converges to select the 702th pairing option. Similarly, Figure 7b demonstrates the time evolution of the sum of the number of bit errors for all users, which is denoted by *system bit error*. We observed that *system bit error* converges to a small value, which is actually zero, after approximately the time step of 1000. That is, the laser chaos decision-maker achieves the optimal pairing, achieving zero *system bit error*.

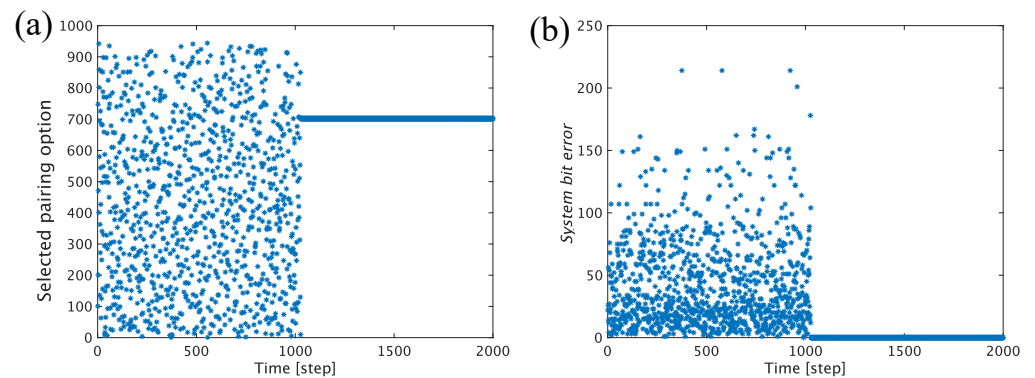


**Figure 7.** Visualization of the behavior of the LCDM-NOMA. (a) Time evolution of the selected pairing option; (b) time evolution of the *system bit error*.

Figure 8 examines performance comparison among C-NOMA, UCGD-NOMA and the proposed method (LCDM-NOMA) with respect to the BER after 2000 steps while modifying the cell size under study. The cell radius is configured from 100 m to 1000 m with a 100 m interval. The number of the threshold level in LCDM-NOMA was specified by  $Z = 1$ . Figure 8 demonstrates that the proposed LCDM-NOMA achieves a smaller BER than the C-NOMA and UCGD-NOMA. Specifically, the LCDM-NOMA can get 99.79% improvement compared to C-NOMA and UCGD-NOMA when the cell radius is 400 m. Therefore, we conclude LCDM-NOMA is better than C-NOMA and UCGD-NOMA concerning BER.

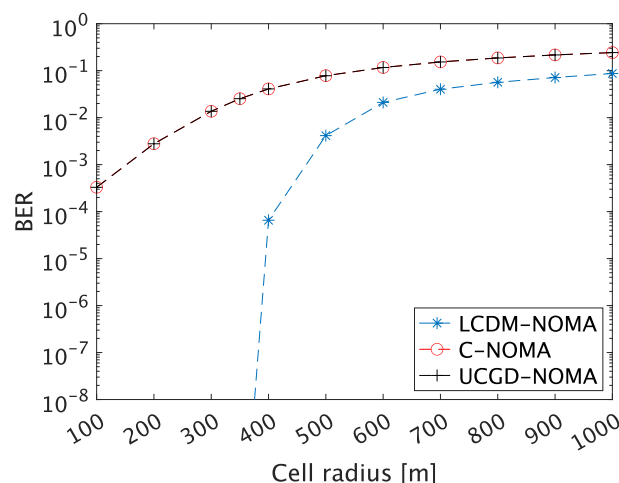


**Figure 8.** Comparison of the LCDM-NOMA with the C-NOMA and the UCGD-NOMA in BER.

## 5. Parameter Optimization for NOMA System with Laser Chaos Decision-Maker and Error Correcting Codes

### 5.1. NOMA System with Error Correcting Codes

Here, we consider introducing error correcting code (ECC) in the system. Error correction capability depends on the type of ECCs. Again, we define the number of bit errors at the  $n$ th user as  $bit-error_n$ . Additionally, we define the  $\varphi$  bit-correctable error

correcting code for the  $n$ th user as  $ECC_{\varphi,n}$ .  $\varphi_n$  is the number of correctable bit errors on the  $n$ th user.  $ECC_{\varphi,n}$  takes various values depending on the type of ECCs.

It should be noted that a user may respond ACK to BS, although bit errors indeed occur. For example, with  $ECC_{0,n}$  for the  $n$ th user, we do not consider error correction because  $ECC_{0,n}$  means 0 bit-correctable error correcting code. That is, for example, in the case of  $bit-error_n = 1$  for the  $n$ th user, when  $ECC_{0,n}$  is set, the  $n$ th user responds NACK to BS. Conversely, when  $ECC_{2,n}$  is set, meaning that 2 bit-correctable error correcting code is employed, the  $n$ th user responds ACK to BS when  $bit-error_n = 1$ . Therefore, we have to investigate the dependency on the type of ECCs.

### 5.2. Performance Evaluation with ECC

We demonstrate the simulation results regarding the dependency on ECC and other parameters related to laser chaos decision-maker.

First, we evaluate the BER with different  $ECC_{\varphi,n}$ . In this simulation,  $ECC_{\varphi,n}$  is configured as either  $ECC_{0,n}$ ,  $ECC_{1,n}$ ,  $ECC_{3,n}$ , or  $ECC_{5,n}$ . In addition, parameter  $Z$ , related to the laser chaos decision-maker, is set to one. The cell radius is varied from 100 to 1000. Figure 9a shows the simulation results. From Figure 9a, we observe BER becomes smaller as the cell radius is smaller. Furthermore, it should be noted that the optimal  $ECC_{\varphi,n}$  differs depending on the cell radius. The setting  $ECC_{0,n}$  performs the best BER when the cell radius is smaller than about 450 m, whereas the setting  $ECC_{0,n}$  cannot perform the best BER when the cell radius is larger than 450 m. That is, here we confirm that an appropriate setting of  $ECC_{\varphi,n}$  does matter.

Next, we evaluate the BER with adaptive  $ECC_{\varphi,n}$ , where  $\varphi$  is set as an adaptive value. The value of  $\varphi$  is defined as the average bit errors of the last  $\tau$  times for user  $n$ . Adaptive  $ECC_{\varphi,n}$  at step  $t$  can be expressed as:  $\varphi = \sum_{i=1}^{t-\tau} \frac{bit-error_n}{\tau}$ . We denote  $ECC_{\tau 5,n}$  as the adaptive  $ECC_{\varphi,n}$  with  $\tau = 5$ , meaning that the ECC is the average bit errors of the last five transmission times for user  $n$ . In this simulation, the parameter  $Z$  for the laser chaos decision-maker is set to one. Figure 9b summarizes the simulation results while changing the cell radius from 100 m to 1000 m. From Figure 9b, with a larger cell radius, we can see that the adaptive ECC method with  $\tau = 7$  accomplishes smaller BER in the NOMA system while  $\tau = 7$  can get smaller BER than other settings. With a smaller cell radius, on the other hand, the setting of  $ECC_{0,n}$  accomplishes the smallest BER.

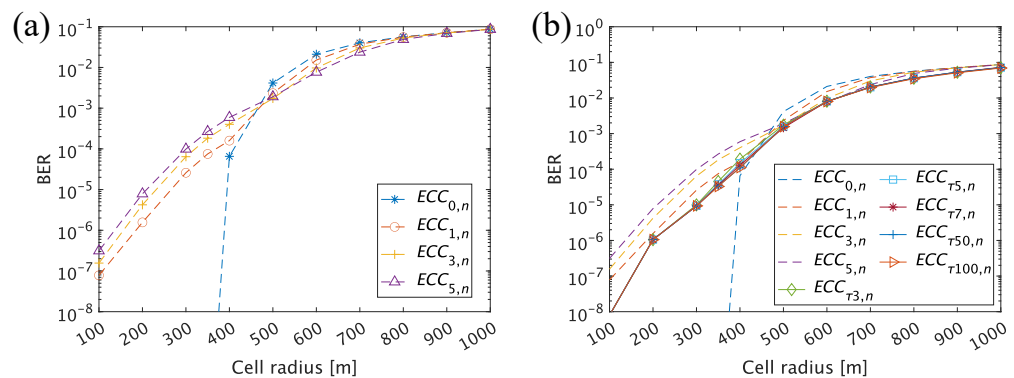


**Figure 9.** BER with different  $ECC_{\varphi,n}$  settings; (a) BER comparison with a fixed ECC. (b) BER comparison with an adaptive ECC.

We also evaluate the effect of the number of thresholds on BER of the proposed LCDM-NOMA. Figure 10 shows simulation results. While maintaining  $\varphi$  being adaptive with  $\tau$  value of 7,  $Z$  is configured differently by 1, 2, 4, 8, 16, 32, 64, and 128. Meanwhile, in the case of  $ECC_{0,n}$ ,  $ECC_{1,n}$ ,  $ECC_{3,n}$ , and  $ECC_{5,n}$ ,  $Z$  is set to 1. Remember that the number of thresholds is given by  $2Z + 1$ . When the number of available threshold levels is small, the threshold can reach the upper or lower limit more quickly. Thus, the convergence of the selection becomes generally fast, whereas accurate selection becomes more difficult.

Conversely, with a larger number of thresholds, it becomes more likely that the threshold reaches its upper or lower limit through sufficient exploration. Hence, the convergence needs a longer time duration but may lead to the correct selection. Figure 10b,c are the enlargement of Figure 10a when the cell radius varies from 100 m to 500 m and from 500 m to 1000 m, respectively. From Figure 10b regarding a smaller cell radius, the BER becomes smaller as the number of thresholds increases. Meanwhile, from Figure 10c with respect to a larger cell radius, the BER becomes smaller as the number of threshold steps is reduced. Therefore, we can conclude that appropriate setting of the number of thresholds improves the system performance depending on the given cell radius. Specifically,  $Z = 4$  is the best when the cell radii are 1000 m and 900 m.  $Z = 8$  is the best when the cell radii are 800 m and 700 m.  $Z = 8$  and  $Z = 64$  are the best when the cell radii are 600 m and 500 m, respectively.  $Z = 128$  and  $Z = 64$  are the best when the cell radii are 400 m and less than 350 m, respectively.

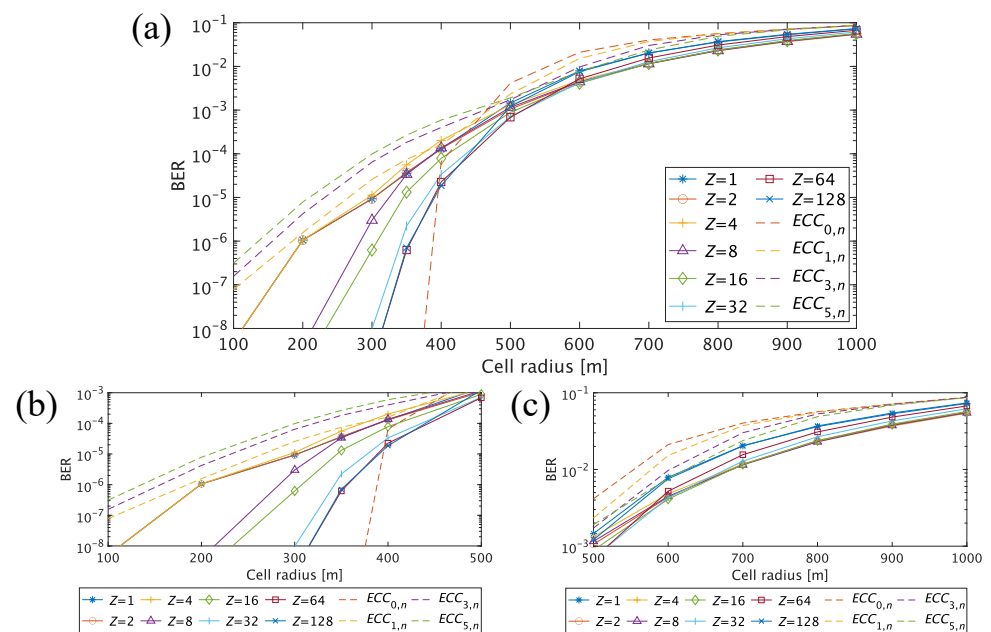


**Figure 10.** (a) BER comparison with the different number of thresholds  $2Z + 1$  related to the laser chaos decision-maker. (ECC is set to  $ECC_{-7}$  for  $Z = 1, \dots, 128$ .  $Z$  is set to 1 for  $ECC_{0,n}$ ,  $ECC_{1,n}$ ,  $ECC_{3,n}$ ,  $ECC_{5,n}$ ). (b) Magnified view of (a) with respect to smaller cell radii; (c) magnified view of (a) with respect to larger cell radii.

### 5.3. Parameter Optimization

Section 5.2 demonstrated that a proper parameter settings of  $ECC_{\varphi,n}$  and  $Z$  indeed works concerning the cell radius in improving the BER performances. Based on these observations, here we introduce another parameter denoted by  $r_n$  that can take three values instead of the former binary (ACK or NACK) to improve the BER performance. When the  $n$ th user experiences zero bit errors, it sends  $r_n = 2$  to the BS. When the number of bit errors is larger than 0 but not larger than  $\varphi_n$ , it sends  $r_n = 1$  to the BS. Finally, when the number of bit errors is larger than  $\varphi_n$ ,  $r_n = 0$  is transmitted to the BS. Namely,  $r_n$  is expressed as follows:

$$r_n = \begin{cases} 2, & \text{if } \text{bit-error}_n = 0. \\ 1, & \text{if } 0 < \text{bit-error}_n \leq \varphi_n. \\ 0, & \text{if } \text{bit-error}_n > \varphi_n. \end{cases} \quad (10)$$

On the BS, ACK or NACK affect the reward as defined before. Since  $r_n$  is set to three values in this case, we define that the selected pairing option wins (i.e., gets a reward) if  $r_n \geq 1$  holds for all  $n$ . Otherwise, the selected pairing option loses (i.e., gets no reward).

We evaluate the performance in terms of BER of the proposed LCDM-NOMA considering parameter optimization via  $r_n$ , and compare it with the case without considering parameter optimization. The solid line in Figure 11 demonstrates the BER when the parameter optimization is employed in LCDM-NOMA, whereas other lines represent the cases without parameter optimization. In the optimization, ECC is also dynamically reconfigured. ECC is given by  $ECC_{\tau 7, n}$  for all users; namely, ECC is adaptively configured with  $\tau = 7$ . Meanwhile,  $Z$  is set, as the best  $Z$  corresponds to the setting of the cell radius before  $\sum_{n=1}^N r_n = 2N$  is satisfied. Once  $\sum_{n=1}^N r_n = 2N$  is achieved, the ECC is set as  $ECC_{0, n}$  while  $Z$  is set as 1. This setting means that ECC is adaptively reconfigured when bit errors are present, whereas once the error-free situation is accomplished, ECC does not look back at past information. From Figure 11, the optimized LCDM-NOMA exhibits lower BER than other cases thanks to the three-valued  $r_n$  and dynamic ECC setting reconfiguration.

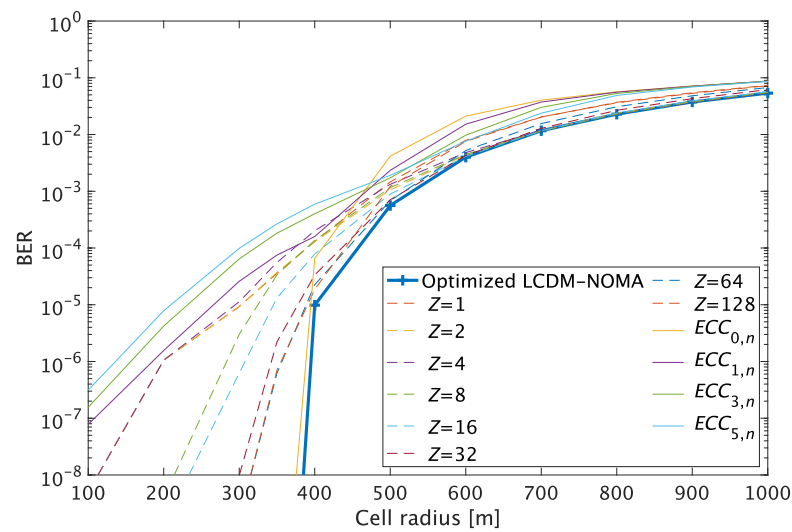


**Figure 11.** Adaptive parameter optimization in LCDM-NOMA. (The thick solid line is the adaptive parameter optimized LCDM-NOMA. The dashed lines with  $Z$  values are based on  $ECC_{\tau 7}$  while using the specified  $Z$  values for the threshold levels. The solid lines with  $ECC_{i, n}$  employ only ACK and NACK in the ECC).

Finally, the optimized LCDM-NOMA is compared with C-NOMA, UCDG-NOMA and an  $\epsilon$ -greedy-based user-pairing scheme. Herein,  $l_v$  and  $s_v$  are defined as the number of selected  $v$ th pairing options and the number of successful communications, respectively. The communication success-rate for the  $v$ th pairing  $p_v$  can be expressed as  $p_v = s_v/l_v$ . In the  $\epsilon$ -greedy-based user pairing scheme, the pair option is selected randomly with probability  $\epsilon$ , and the pairing option with the highest communication success rate with probability  $1 - \epsilon$  is selected. In other words, the pairing option is selected regardless of the communication success rate with probability  $\epsilon$ , and the pairing option which has the highest value of  $p_v$  with probability  $1 - \epsilon$  is selected. We evaluate two cases of  $\epsilon$  by 0.1 and 0.01. From Figure 12, it is remarkable that the optimized LCDM-NOMA exhibits the smallest BER when the cell radius is small compared with other strategies. The reason that our proposed scheme is better than the others can be summarized as follows. C-NOMA and UCGD-NOMA are fixed pairing schemes, which pair users based on their location information without considering BER. On the other hand, our proposed LCDM-NOMA can pair the users based on ACK information that depends on BER by updating the threshold scheme according to the real communication process. Hence, our proposed scheme can pair users with smaller BER compared to C-NOMA and UCGD-NOMA. Moreover, compared to  $\epsilon$ -greedy based scheme, our proposed LCDM-NOMA scheme can search for pairing options more efficiently, by which pairing options with smaller BER can be decided by the BS. Specifically, when the cell radius is 400 m, our proposed optimized LCDM-NOMA scheme can get 99.97% improvement compared to C-NOMA and UCGD-NOMA and



99.41% improvement compared to the epsilon greedy-based user-pairing scheme. In the meantime, the BER performances do not show evident differences among the strategies when the cell radius is large. We speculate that the pairing may not be too difficult in situations where the users are spatially sparsely distributed when the cell radius is large, leading to negligible performance differences among the strategies.

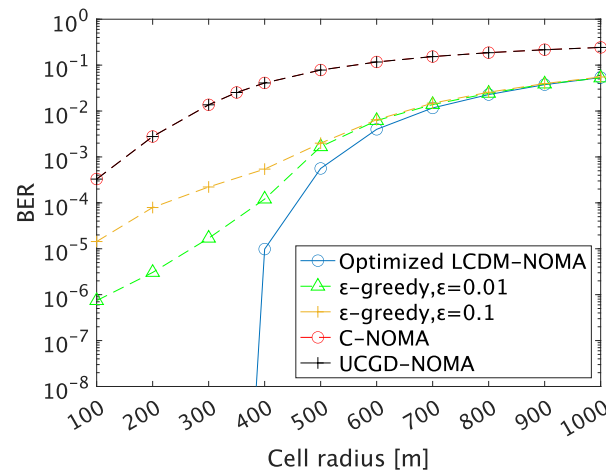


Figure 12. BER comparison with C-NOM, UCGD-NOMA, and  $\epsilon$ -greedy-based user pairing scheme.

## 6. Conclusions

In this study, to achieve fast user pairing for realistic downlink NOMA systems, we designed a user pairing scheme based on a laser chaos decision-maker. In our proposed scheme, the user pairing is accomplished by the laser-chaos-based decision-making algorithm based on responses from the users, reflecting the bit errors using a realistic system model. Simulation results showed that our proposed LCDM-NOMA scheme exhibits superior BER performances compared to conventional methods. Moreover, to improve the performance in terms of BER for our proposed scheme, error-correcting codes are introduced in the system. Furthermore, parameter dependencies in the user pairing by a laser chaos decision-maker are investigated to minimize the BER of the NOMA system. We demonstrated that error-correcting codes and the fine or coarse tuning of decision-making impact the system performance depending on the cell radius. Moreover, simulation results demonstrated that our proposed scheme considering error-correcting mechanisms exhibits superior performances in BER compared to other conventional schemes. As the cell radius of the NOMA system gets smaller, the superior on the BER of our proposed scheme gets bigger. Specifically, our proposed scheme can decrease the BER from  $10^{-1}$  to  $10^{-5}$  compared to the conventional schemes when the cell radius is 400m. Based on these insights, we demonstrated an adaptive pairing scheme to optimize operation parameters to minimize BER of the NOMA system under study. Further adaptive principles are of interest for future studies, including adaptive modulation format and resource block assignments as well as experimental demonstrations.

**Author Contributions:** Conceptualization, A.L., M.N. and M.H.; methodology, M.S., A.L., Z.D., M.N. and M.H.; software, M.S., A.L. and Z.D.; validation, M.S.; formal analysis, M.S., A.L., M.N. and M.H.; investigation, M.S., A.L., Z.D., M.N. and M.H.; resources, M.S., A.L. and M.H.; data curation, M.S.; writing—original draft preparation, M.S.; writing—review and editing, A.L., M.N. and M.H.; visualization, M.S. and A.L.; supervision, A.L., M.N. and M.H.; project administration, M.N. and M.H.; funding acquisition, A.L., M.N. and M.H. All authors have read and agreed to the published version of the manuscript.

**Funding:** This work was supported partly by the CREST project (JPMJCR17N2) funded by the Japan Science and Technology Agency and Grants-in-Aid for Scientific Research (JP20H00233) funded by the Japan Society for the Promotion of Science.

**Conflicts of Interest:** The authors declare no conflict of interest.

## References

1. Abrardo, A.; Moretti, M.; Saggese, F. Power and Subcarrier Allocation in 5G NOMA-FD Systems. *IEEE Trans. Commun.* **2020**, *19*, 8246–8260. [\[CrossRef\]](#)
2. Chen, X.; Gong, F.; Li, G.; Zhang, H.; Song, P. User Pairing and Pair Scheduling in Massive MIMO-NOMA Systems. *IEEE Commun. Lett.* **2018**, *22*, 788–791. [\[CrossRef\]](#)
3. Krishnamoorthy, A.; Schober, R. Uplink and Downlink MIMO-NOMA with Simultaneous Triangularization. *IEEE Trans. Wirel. Commun.* **2021**, *20*, 3381–3396. [\[CrossRef\]](#)
4. Jia, M.; Gao, Q.; Guo, Q.; Gu, X. Energy-Efficiency Power Allocation Design for UAV-Assisted Spatial NOMA. *IEEE Internet Things J.* **2021**, *8*, 15205–15215. [\[CrossRef\]](#)
5. Islam, S.M.R.; Avazov, N.; Dobre, O.A.; Kwak, K. Power-Domain Non-Orthogonal Multiple Access (NOMA) in 5G Systems: Potentials and Challenges. *IEEE Commun. Surv. Tutor.* **2017**, *19*, 721–742. [\[CrossRef\]](#)
6. Yang, G.; Xu, X.; Liang, Y.-C.; Di Renzo, M. Reconfigurable Intelligent Surface-Assisted Non-Orthogonal Multiple Access. *IEEE Trans. Wirel. Commun.* **2021**, *20*, 3137–3151. [\[CrossRef\]](#)
7. Abuajwa, O.; Roslee, M.B.; Yusoff, Z.B. Simulated Annealing for Resource Allocation in Downlink NOMA Systems in 5G Networks. *Appl. Sci.* **2021**, *11*, 4592. [\[CrossRef\]](#)
8. Cai, D.; Ding, Z.; Fan, P.; Yang, Z. On the Performance of NOMA with Hybrid ARQ. *IEEE Trans. Veh. Technol.* **2018**, *67*, 10033–10038. [\[CrossRef\]](#)
9. Xu, Y.; Cai, D.; Fang, F.; Ding, Z.; Shen, C.; Zhu, G. Outage Constrained Power Efficient Design for Downlink NOMA Systems with Partial HARQ. *IEEE Trans. Commun.* **2020**, *68*, 5188–5201. [\[CrossRef\]](#)
10. Panchal, A.; Dutta, A.K. Performance Analysis and Design of MIMO Power NOMA with Estimated Parameters Error Statistics Along with SIC and Hardware Imperfections. *IEEE Trans. Veh. Technol.* **2021**, *70*, 1488–1500. [\[CrossRef\]](#)
11. Kishore, R.; Gurugopinath, S.; Muhaidat, S.; Bouanani, F.E.; Dobre, O.A. Sum Rate Analysis of Generalized Space Shift Keying-Aided MIMO-NOMA Systems. *IEEE Trans. Veh. Technol.* **2021**, *70*, 7232–7236. [\[CrossRef\]](#)
12. Shahab, M.B.; Kade, M.F.; Shin, S.Y. A Virtual User Pairing Scheme to Optimally Utilize the Spectrum of Unpaired Users in Non-orthogonal Multiple Access. *IEEE Signal Process. Lett.* **2016**, *23*, 1766–1770. [\[CrossRef\]](#)
13. Mouni, N.S.; Kumar, A.; Upadhyay, P.K. Adaptive User Pairing for NOMA Systems with Imperfect SIC. *IEEE Wirel. Commun. Lett.* **2021**, *10*, 1547–1551. [\[CrossRef\]](#)
14. He, C.; Hu, Y.; Chen, Y.; Zeng, B. Joint Power Allocation and Channel Assignment for NOMA with Deep Reinforcement Learning. *IEEE J. Sel. Areas Commun.* **2019**, *37*, 2200–2210. [\[CrossRef\]](#)
15. Mouchili, S.; Hamouda, S. Pairing Distance Resolution and Power Control for Massive Connectivity Improvement in NOMA Systems. *IEEE Trans. Veh. Technol.* **2020**, *69*, 4093–4103. [\[CrossRef\]](#)
16. Duan, Z.; Li, A.; Okada, N.; Ito, Y.; Chauvet, N.; Naruse, M.; Hasegawa, M. User Pairing Using Laser Chaos Decision Maker for NOMA Systems. *Nonlinear Theory Appl.* **2022**, *13*, 72–83. [\[CrossRef\]](#)
17. Zhu, L.; Zhang, J.; Cao, X.; Wu, D.O. Optimal User Pairing for Downlink Non-Orthogonal Multiple Access (NOMA). *IEEE Wirel. Commun. Lett.* **2019**, *8*, 328–331. [\[CrossRef\]](#)
18. Chahab, M.B.; Irfan, M.; Kader, M.F.; Shin, S.Y. User pairing schemes for capacity maximization in non-orthogonal multiple access systems. *Wirel. Commun. Mob. Comput.* **2016**, *16*, 2884–2894.
19. Mouchili, S.; Hamouda, S. New User Grouping Scheme for Better User Pairing in NOMA Systems. In Proceedings of the International Wireless Communications and Mobile Computing (IWCMC), Limassol, Cyprus, 15–19 June 2020; pp. 820–825.
20. Lee, J.; So, J. Reinforcement Learning-Based Joint User Pairing and Power Allocation in MIMO-NOMA Systems. *Sensors* **2020**, *20*, 7094. [\[CrossRef\]](#) [\[PubMed\]](#)
21. Wang, S.; Lv, T.; Ni, W.; Beaulieu, N.C.; Guo, Y.J. Joint Resource Management for MC-NOMA: A Deep Reinforcement Learning Approach. *IEEE Trans. Wirel. Commun.* **2021**, *20*, 5672–5688. [\[CrossRef\]](#)
22. Rezwan, S.; Choi, W. Priority-Based Joint Resource Allocation with Deep Q-Learning for Heterogeneous NOMA Systems. *IEEE Access* **2021**, *9*, 41468–41481. [\[CrossRef\]](#)
23. Zhang, H.; Zhang, H.; Long, K.; Karagiannidis, G.K. Deep Learning Based Radio Resource Management in NOMA Networks: User Association, Subchannel and Power Allocation. *IEEE Trans. Netw. Sci. Eng.* **2020**, *7*, 2406–2415. [\[CrossRef\]](#)
24. Gui, G.; Huang, H.; Song, Y.; Sari, H. Deep Learning for and Effective Nonorthogonal Multiple Access Scheme. *IEEE Trans. Veh. Technol.* **2018**, *67*, 8440–8450. [\[CrossRef\]](#)
25. Shastri, B.J.; Tait, A.N.; de Lima, T.F.; Pernice, W.H.; Bhaskaran, H.; Wright, C.D.; Prucnal, P.R. Photonics for artificial intelligence and neuromorphic computing. *Nat. Photonics* **2021**, *15*, 102–114. [\[CrossRef\]](#)
26. Chen, Z.; Segev, M. Highlighting photonics: Looking into the next decade. *eLight* **2021**, *1*, 2. [\[CrossRef\]](#)
27. Genty, G.; Salmela, L.; Dudley, J.M.; Brunner, D.; Kokhanovskiy, A.; Kobtsev, S.; Turitsyn, S.K. Machine learning and applications in ultrafast photonics. *Nat. Photonics* **2021**, *15*, 91–101. [\[CrossRef\]](#)
28. Kitayama, K.; Notomi, M.; Naruse, M.; Inoue, K.; Kawakami, S.; Uchida, A. Novel frontier of photonics for data processing—Photonic accelerator. *APL Photonics* **2019**, *4*, 090901. [\[CrossRef\]](#)
29. Uchida, A. *Optical Communication with Chaotic Lasers: Applications of Nonlinear Dynamics and Synchronization*; Wiley-VCH: Weinheim, Germany, 2012.

30. Naruse, M.; Terashima, Y.; Uchida, A.; Kim, S.-J. Ultrafast photonic reinforcement learning based on laser chaos. *Sci. Rep.* **2017**, *7*, 8772. [[CrossRef](#)]
31. Naruse, M.; Mihana, T.; Hori, H.; Saigo, H.; Okamura, K.; Hasegawa, M.; Uchida, A. Scalable photonic reinforcement learning by time-division multiplexing of laser chaos. *Sci. Rep.* **2018**, *8*, 10890. [[CrossRef](#)]
32. Naruse, M.; Chauvet, N.; Uchida, A.; Drezet, A.; Bachelier, G.; Huant, S.; Hori, H. Decision Making Photonics: Solving Bandit Problems Using Photons. *IEEE J. Sel. Top. Quantum Electron.* **2019**, *26*, 7700210. [[CrossRef](#)]
33. Okada, N.; Hasegawa, M.; Chauvet, N.; Li, A.; Naruse, M. Analysis on Effectiveness of Surrogate Data-Based Laser Chaos Decision Maker. *Complexity* **2021**, *2021*, 8877660. [[CrossRef](#)]
34. Furukawa, H.; Li, A.; Shoji, Y.; Watanabe, Y.; Kim, S.J.; Sato, K.; Andreopoulos, Y.; Hasegawa, M. A Channel selection algorithm using reinforcement learning for mobile devices in massive IoT system. In Proceedings of the 2021 IEEE 18th Annual Consumer Communications & Networking Conference (CCNC), Virtual, 9–12 January 2021.
35. Takeuchi, S.; Hasegawa, M.; Kano, K.; Uchida, A.; Chauvet, N.; Naruse, M. Dynamic channel selection in wireless communications via a multi-armed bandit algorithm using laser chaos time series. *Sci. Rep.* **2020**, *10*, 1574. [[CrossRef](#)]
36. Kanemasa, H.; Li, A.; Naruse, M.; Chauvet, N.; Hasegawa, M. Dynamic channel bonding in WLANs by hierarchical laser chaos decision maker. *Nonlinear Theory Appl.* **2022**, *13*, 84–100. [[CrossRef](#)]
37. Li, A.; Fujisawa, M.; Urabe, I.; Kitagawa, R.; Kim, S.J.; Hasegawa, M. A lightweight decentralized reinforcement learning based channel selection approach for high-density LoRaWAN. In Proceedings of the 2021 IEEE International Symposium on Dynamic Spectrum Access Networks (DySPAN), Virtual, 13–15 December 2021.
38. Yahya, H.; Alsusa, E.; Al-Dweik, A. Exact BER Analysis of NOMA with Arbitrary Number of Users and Modulation Orders. *IEEE Trans. Commun.* **2021**, *69*, 6330–6344. [[CrossRef](#)]
39. Otsuka, T.; Kurasawa, K.; Duan, Z.; Li, A.; Sato, K.; Takesue, H.; Aihara, K.; Inaba, K.; Hasegawa, M. Coherent Ising Machine Based Optimal Channel Allocation and User Pairing in NOMA Networks. In Proceedings of the 2021 International Conference on Artificial Intelligence in Information and Communication (ICAIIIC), Virtual, 13–16 April 2021.